Cell size, cell cycle, and α-smooth muscle actin expression by primary human lung fibroblasts

Bruce D. Uhal, Carlos Ramos, Iravati Joshi, Antonio Bifero, Annie Pardo and Moises Selman

Am J Physiol Lung Cell Mol Physiol 275:L998-L1005, 1998.

Cell size, cell cycle, and α-smooth muscle actin expression by primary human lung fibroblasts

BRUCE D. UHAL,[1] CARLOS RAMOS,[2] IRAVATI JOSHI,[1] ANTONIO BIFERO,[1] ANNIE PARDO,[3] AND MOISES SELMAN[2]

[1]*Lung Cell Kinetics Laboratory and The Cardiovascular Institute, Michael Reese Hospital, Chicago, Illinois 60616; and* [3]*Facultad de Ciencias, Universidad Nacional Autonoma de Mexico, Coyoacan 04000; and* [2]*Instituto Nacional de Enfermedades Respiratorias, Tlalpan 14080, Mexico*

Uhal, Bruce D., Carlos Ramos, Iravati Joshi, Antonio Bifero, Annie Pardo, and Moises Selman. Cell size, cell cycle, and α-smooth muscle actin expression by primary human lung fibroblasts. *Am. J. Physiol.* 275 (*Lung Cell. Mol. Physiol.* 19): L998–L1005, 1998.—Primary human lung fibroblasts were separated into small (*group I*), intermediate (*group II*), and large (*group III*) subpopulations by unit gravity sedimentation (1 G). The three subsets retained differences in cell size for up to 15 days of primary culture. Flow cytometric (fluorescence-activated cell sorter) measurements of forward-angle light scatter agreed well with fibroblast volume measured by image analysis and confirmed the utility of forward-angle light scatter for discriminating size subpopulations. *Group II* fibroblasts accumulated most rapidly by 8 days of culture and also contained the greatest proportion of S and G_2/M phase cells as determined by fluorescence-activated cell sorter. Fibroblasts that were immunoreactive with antibodies to α-smooth muscle actin (α-SMA) were found only in *group III*. In situ end labeling of fragmented DNA detected apoptotic cells in both *groups II* and *III*, but double labeling for in situ end labeling and α-SMA revealed apoptotic cells in both the α-SMA-positive and -negative populations. These results demonstrate that primary human lung fibroblasts behave as predicted by classic models of cell cycle progression and differentiation. However, they do not support the hypothesis that the expression of α-actin is related to apoptosis. We also describe a simple and reproducible method for the high-yield isolation of human lung fibroblast subsets of differing proliferative potential and phenotype.

lung cells; myofibroblast; apoptosis; proliferation; cell heterogeneity

LUNG FIBROBLAST SUBPOPULATIONS of functionally distinct capacities have been isolated from rodent and human tissues. From the mouse lung, two subpopulations have been identified by disparate expression of the allelic antigen Thy 1 (15, 16). Subpopulations of human lung fibroblasts also have been discriminated on the basis of expression of the receptor for the complement subcomponent C1q (1). Fibroblastic foci in the lungs of patients with interstitial lung disease contain fibroblasts of the subtype termed VA, which was identified by expression of the intermediate filaments vimentin and α-smooth muscle actin (α-SMA) (12). The VA subpopulation is but one member of the myofibroblast phenotype, a heterogeneous family of mesenchymal cells observed in a variety of injured and/or repairing tissues (9, 18).

Investigations of primary isolates of these fibroblast subsets have revealed differences in growth rate (17), collagen synthesis (5), and responses to various cytokines (26). On this basis, it is believed that the initial distribution and subsequent selection of these subpopulations is likely a critical determinant in the pathogenesis and/or resolution of pulmonary fibrosis (8). In vitro, these fibroblast subpopulations exhibit reproducible patterns of morphology. Fibroblast subsets of mouse lung, when cultured after separation by fluorescence-activated cell sorter (FACS) analysis of Thy 1 expression, displayed either a spindle-shaped morphology with lipid inclusion bodies or a larger and more rounded morphology (15). Similarly, human lung fibroblast subsets separated by C1q-receptor expression also displayed two distinct morphologies: spindle-shaped cells with elongated processes (high binding) or larger and more flattened cells (1).

The large and flat fibroblast morphology was also observed in cultures of microfilament-laden myofibroblasts isolated from experimental granulating wounds inflicted on rats (23). In studies of mouse and human lung cells in vitro (1, 17), the large and flat fibroblast subsets were found to grow more slowly in culture than those with the smaller spindle shape. Myofibroblasts isolated from connective tissue stroma of human breast carcinomas or from associated granulating wounds also grew more slowly than fibroblasts obtained from normal human tissue (24). The finding of markers of apoptosis within myofibroblast populations in vivo (7) has led to the speculation that fibroblast differentiation to the myofibroblast phenotype might represent a terminal pathway leading to apoptosis (6).

Together, these observations suggest an interdependence of lung fibroblast phenotype and cell cycle progression. An understanding of this relationship might provide new insights into lung fibroblast function as well as new tools for future investigations. To begin studying this topic, we hypothesized that a simple cell separation protocol based on differences in cell size would also discriminate fibroblast subsets of functionally distinct capacities, particularly with respect to growth kinetics. We describe here the application of unit gravity sedimentation (1 G) as a cell separation method for human fibroblasts isolated from normal lung tissue, and we report the resolution of size subpopulations of high yield and disparate proliferation kinetics. Initial evaluations of these subsets are consistent

The costs of publication of this article were defrayed in part by the payment of page charges. The article must therefore be hereby marked "*advertisement*" in accordance with 18 U.S.C. Section 1734 solely to indicate this fact.

with classic models of cell size and cell cycle progression and suggest that expression of the myofibroblast phenotype is unrelated to the commitment to apoptosis.

METHODS

Materials. Materials for cell isolation and culture were purchased from sources described elsewhere (22). Propidium iodide, trypsin, trypsin inhibitor, avidin-rhodamine, and an FITC-conjugated monoclonal antibody to α-SMA were obtained from Sigma (St. Louis, MO). Avidin-FITC, both FITC- and rhodamine-conjugated anti-mouse IgGs, and DNase-free RNase, cytometry grade, were purchased from Boehringer Mannheim (Indianapolis, IN). Fluorescein-conjugated annexin V was obtained from PharMingen (San Diego, CA). All other chemicals were of reagent grade.

Fibroblast isolation and culture. Primary lung fibroblasts were isolated at the National Institute of Respiratory Diseases (Tlalpan, Mexico) from a patient undergoing a lobectomy for removal of a primary lung tumor (14). No morphological evidence of disease was found in the tissue samples used for fibroblast isolation. The cells were isolated by trypsin dispersion as described earlier (14), and fibroblast strains were established in Dulbecco's modified Eagle's medium (or in Ham's F-12 medium) supplemented with 10% fetal bovine serum (FBS), 200 U/ml of penicillin, and 200 mg/ml of streptomycin. All cells were cultured at 37°C in 95% air-5% CO_2 until early confluence. One early-passage strain (N12, *passage 10*) was chosen arbitrarily for this study. Cell number was determined with the cell proliferation reagent WST-1 (Boehringer Mannheim), a tetrazolium salt cleaved by the mitochondria of viable cells to yield a soluble formazan chromophore. Relative cell density was determined according to the instructions provided by the manufacturer. In a pilot study, WST-1 absorbance was proportional to cell number as determined by hemocytometer counts. In addition, no significant differences were found in the WST-1 absorbances for small (*group I*), intermediate (*group II*), or large (*group III*) fibroblasts assayed at equivalent cell numbers predetermined by hemocytometer (data not shown). Thus the determination of cell accumulation rates with WST-1 was unaffected by the differences in cell size between *group I*, *II*, and *III* fibroblasts.

Unit gravity sedimentation. Fibroblast separation on the basis of cell size was conducted as described earlier for type II alveolar epithelial cells (19, 20). Briefly, $5–10 \times 10^6$ fibroblasts were trypsinized, washed, and resuspended in 50 ml of Ham's F-12 medium buffered with HEPES and containing 2% FBS. The suspension was layered over an eight-step discontinuous gradient of Ficoll (2–8% wt/vol, 50 ml/step) in Ham's F-12 medium containing 2% FBS and buffered with HEPES at pH 7.3, all in a 4°C cold room. The gradient chamber was slowly lowered over a period of 20 min to the horizontal position (15), where it remained for 60 min. The chamber was then returned to a vertical position over 20 min, and 36 fractions of 15 ml each were collected through a port in the chamber bottom. The cells were either fixed immediately with 70% ethanol (22) or recovered for subsequent culture in Ham's F-12 medium containing 10% FBS. Over five separate experiments, as many as 20×10^6 cells or as few as 3×10^6 cells were separated, with no change in light scatter or volume profiles of the resulting pooled groups.

Flow cytometry. Flow cytometric analyses were performed on a Partec CA-III flow cytometer equipped with a 25-mW argon ion laser for excitation at 488 nm. Propidium iodide and rhodamine (tetramethylrhodamine isothiocyanate) fluorescences were acquired through a 610-nm long-pass filter and fluorescein (FITC) fluorescence was acquired through an EM520 band-pass filter. After standardization with fluorescent microspheres (Coulter, Hialeah, FL), amplifier gains were not changed throughout an experiment. Preparation of cells for DNA distribution and 5-bromo-2′-deoxyuridine (BrdU) incorporation experiments was conducted as described earlier (22), with cell fixation in 70% ethanol followed by incubations with 4 N HCl and DNase-free RNase. For analysis of apoptosis by in situ end labeling (ISEL) (25), the cells were labeled with biotinylated dUTP. Depending on experimental requirements, biotinylated DNA was detected with avidin-FITC or avidin-rhodamine essentially as described by Gorczyca et al. (10).

For analyses of apoptosis by annexin V binding, the cells were trypsinized from culture dishes and incubated for 1 h in suspension. Fluorescein-conjugated annexin V was added to the medium for 15 min at the concentration recommended by the supplier, after which the cells were washed and resuspended in PBS for immediate FACS analysis. For immunocytochemistry, fibroblasts were fixed with ice-cold 70% ethanol and stored at −20°C until assay. The cells were washed and incubated for 1 h at 37°C with FITC-conjugated monoclonal anti-human α-SMA antibody diluted 1:400 in 1% bovine serum albumin in PBS, pH 7.3. The cells were washed and resuspended in PBS for FACS analysis. Fluorescence and forward-angle light scatter (FALS) data were acquired in linear or log scale as indicated in Figs. 2–5 and 8. Flow cytometric data were analyzed and quantitated with WINMDI software (Scripps Institute, La Jolla, CA) with the Quandrant Statistics routine for compartmentation of bivariate histograms. When visual compartmentation of the histograms was not possible, the histogram subtraction function of MULTI2D software (Phoenix Flow Systems, San Diego, CA) was used. Univariate DNA distribution data were compartmented into cell cycle phase fractions with the software MULTICYCLE (Phoenix Flow Systems); doublets were eliminated from the compartmentation computations through software-resident curve-fitting algorithms based on 2N versus 4N peak position.

Microscopy and image analysis. Photomicroscopy was performed on an Olympus EMT-2 epifluorescence-phase-contrast microscope equipped with band-pass filters for detection of FITC and rhodamine-propidium iodide, respectively, and fitted with both color and gray-scale charge-coupled device cameras. Cell volume was determined by automated measurement of the ferret diameters of each of 50 cells/group with the image-analysis program MOCHA (Jandel Scientific, San Rafael, CA). The ferret diameters were converted to cell volumes by calculation. Quantitation of fluorescence images was performed through intensity thresholding and pixel summation algorithms resident in the MOCHA image-analysis software.

RESULTS

Fibroblast size and light-scatter profile. Unit gravity sedimentation (1 G) over an eight-step gradient of Ficoll clearly resolved fibroblast subsets on the basis of cell size. The most extreme differences in cell size were observed between pooled gradient *fractions 1–6* (Fig. 1*A*) and *25–30* (Fig. 1*B*) immediately after removal from the sedimentation chamber. The size difference was also evident after 1 (Fig. 1, *C* and *D*) and 15 days (Fig. 1, *E* and *F*) of subsequent culture. At culture *day 1*, the large cells were generally of the "stellate" morphology and the small cells were primarily "spindle" shaped; these phenotypes still differed in size on culture *day 15* (see *Fibroblast size and proliferation kinetics*).

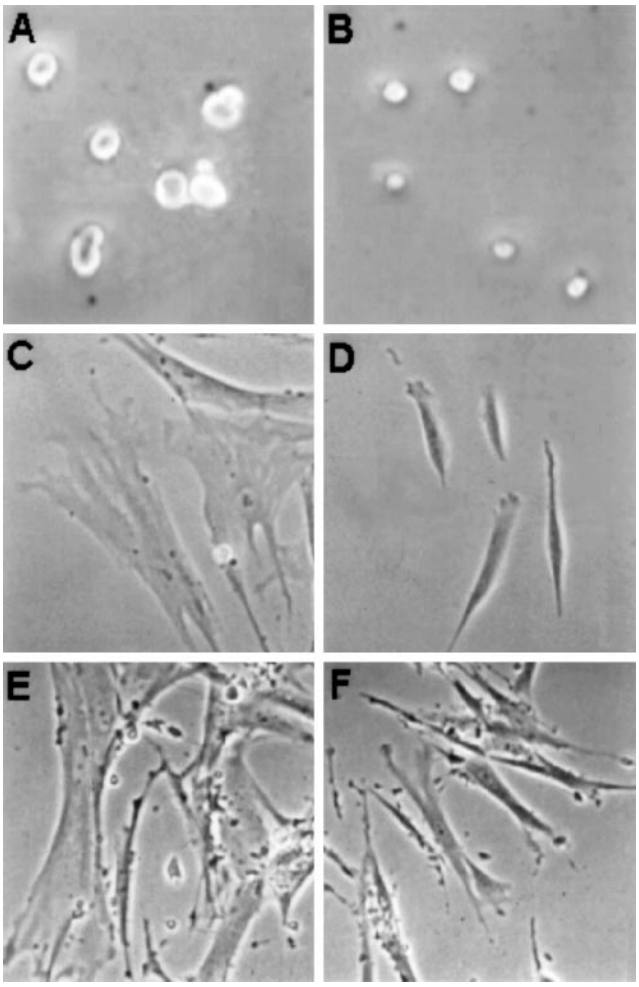

Fig. 1. Phase-contrast microscopy of human lung fibroblast subpopulations separated by unit gravity sedimentation (1 G). Relative size differences were readily apparent in fibroblasts immediately after pooling of Ficoll gradient *fractions 1–6* (*A*) and *25–30* (*B*). Size gradient of the same subsets was also evident after 1 (*C* and *D*, respectively) and 15 (*E* and *F*, respectively) days of primary culture. Quantitation of cell volume in pooled gradient fractions is reported in Fig. 3.

Comparison of pooled gradient *fractions 1–6* and *25–30* also revealed the most extreme differences in light-scatter intensity. Figure 2 displays FALS profiles for *fractions 1–6* and *25–30* measured in conjunction with nuclear DNA content by propidium iodide binding (22). Although heterogeneity of light-scatter intensity was evident in each sample, median FALS values were reproducible and easily measured. The N12 fibroblast strain did not contain lipid inclusion bodies detectable by phase-contrast microscopy or Oil Red O staining (data not shown), and thus the light-scatter profiles of these cells were not influenced by the presence of lipid-filled organelles. The small bodies visible by light microscopy after time in culture (Fig. 1, *E* and *F*) were removed by washing and thus were not intracellular.

Figure 3 plots the median FALS values for each of five pooled gradient fractions as a function of cell volume measured by static-image cytometry. With the exception of the smallest group of fibroblasts (*fractions*

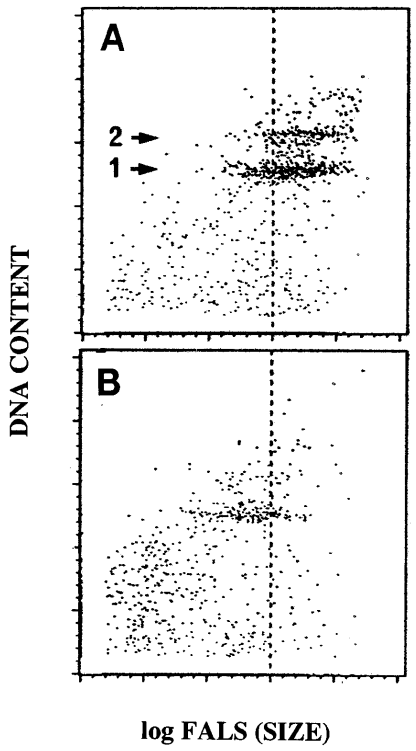

Fig. 2. Flow cytometric [fluorescence-activated cell sorter (FACS)] analysis of light scatter and ploidy of human fibroblast subsets separated by 1 G. Immediately after separation, cells in pooled Ficoll gradient *fractions 1–6* (*A*) and *25–30* (*B*) were fixed in ethanol and subjected to FACS analysis of forward-angle light scatter (FALS) vs. DNA content as previously described (19, 22). *1* and *2*, diploid (G_0/G_1 phase) and tetraploid (G_2/M phase) fibroblast populations, respectively, as detected by propidium iodide fluorescence of RNase-treated cells. Quantitation of cell cycle phase fractions is reported in Fig. 4 and text. Compare *x*-axis position of *populations 1* and *2* relative to constant FALS marker at channel 150 (dotted line).

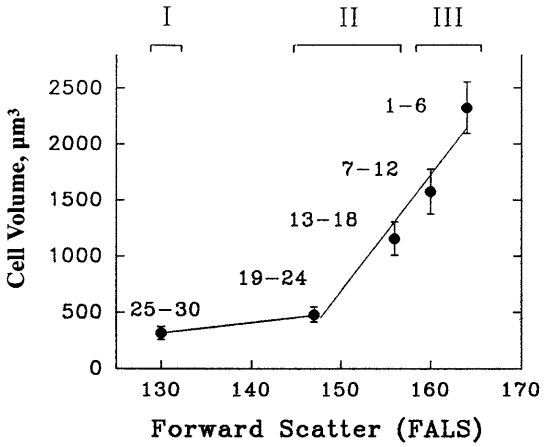

Fig. 3. Relationship of cell volume and FALS in ethanol-fixed human lung fibroblasts. Immediately after separation, cells in pooled Ficoll gradient *fractions 1–6*, *7–12*, *13–18*, *19–24*, and *25–30* were fixed in ethanol and subjected to FACS analysis of FALS (plotted in log scale) as described in Fig. 2. Average cell volume was determined by static image analysis of the same samples used for FACS (see METHODS). Each point is mean ± SD of cell volume and median FALS channel for pooled fraction. Line between *fractions 19–24* and *1–6* is linear regression ($r = 0.94$). For subsequent experiments, isolated fractions were combined into *groups I* (small cells; *fractions 25–30*), *II* (medium cells; *fractions 13–24*), and *III* (large cells; *fractions 1–12*).

25–30), the diameter of which approached that of bare nuclei (7.3 ± 0.6-μm nuclear diameter vs. 8.44 ± 2.5-μm cell diameter), the median FALS value correlated well with average cell volume ($r = 0.94$). On the basis of this plot, all subsequent measurements were made on either unfractionated cells or Ficoll gradient fractions pooled into small (*group I, fractions 25–30*), intermediate (*group II, fractions 13–24*), and large (*group III, fractions 1–12*) fibroblast subsets. In three experiments, the percentage of total cells recovered in each of the three groups ranged from 23 to 28% (*group I*), 38 to 42% (*group II*), and 30 to 39% (*group III*).

Fibroblast size and proliferation kinetics. DNA distribution data obtained by analyses of propidium iodide binding (see Fig. 2) were compartmented by established methods (22) to yield cell cycle phase fractions for each fibroblast group. As shown in Fig. 4, *group II* contained the highest percentage of S and G_2/M phase cells, roughly threefold higher than that of the unfractionated fibroblast strain. *Groups I* and *III* exhibited cell cycle phase distributions of 82, 3, and 15% and 85, 4, and 11% for G_0/G_1, S, and G_2/M phases, respectively, distributions essentially identical to the unfractionated N12 strain. In addition, bivariate analysis of FALS and the thymidine analog BrdU incorporated into the DNA of viable S phase cells (5) revealed that BrdU incorporation was confined to fibroblasts of intermediate size

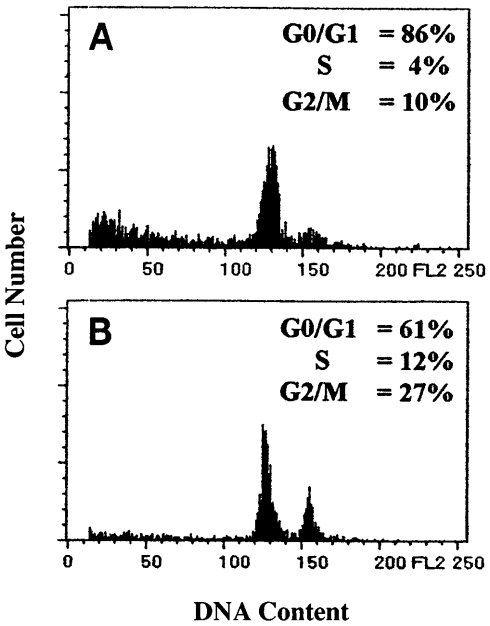

Fig. 4. DNA distribution analysis of fibroblast subsets separated by 1 G. Ethanol-fixed fibroblasts were incubated with 5 μg/ml of propidium iodide and DNase-free RNase for ploidy analysis by FACS as described earlier (22). DNA distributions displayed are from unfractionated (*A*) and *group II* (*B*) fibroblasts defined in Fig. 3. *Inset*, percentage of cells in each cell cycle phase. *Groups I* and *III* exhibited percent distributions nearly identical to unfractionated cells (see text). Experiment was performed twice with similar results. For the 2 experiments, ranges of cell cycle distributions were 81–86% G_0/G_1, 4–7% S, and 10–12% G_2/M for unfractionated cells; 55–61% G_0/G_1, 12–19% S, and 26–27% G_2/M for *group II*; 82–84% G_0/G_1, 4–6% S, and 10–12% G_2/M for *group I*; and 80–85% G_0/G_1, 3–7% S, and 8–13% G_2/M for *group III*.

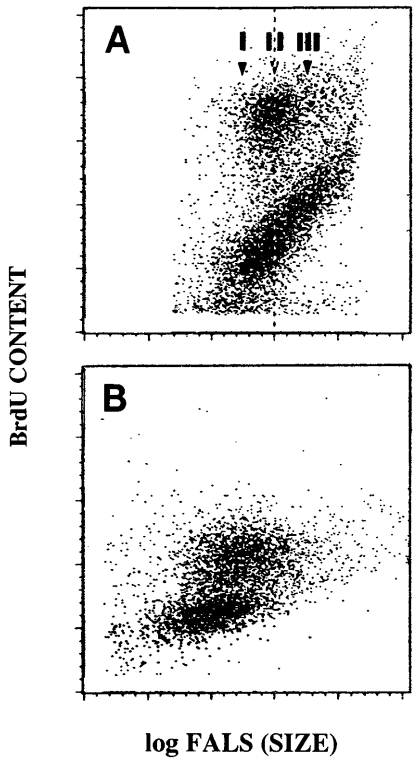

Fig. 5. Relationship of human lung fibroblast size to incorporation of 5-bromo-2′-deoxyuridine (BrdU). Unfractionated primary N12 human lung fibroblasts (*A*) and A549 human lung carcinoma cell line (*B*) were cultured to mid-log phase and were incubated for 1 h with 10 μM BrdU. Cells were then harvested for FACS detection of incorporated BrdU (22) vs. cell size measured as FALS. Note midrange FALS intensity of BrdU-positive N12 fibroblasts (*A, top*) and contrast that with A549 BrdU-positive subset of high-FALS intensity relative to unlabeled population. Arrowheads, median FALS values for each group.

(Fig. 5). This was in contrast to BrdU incorporation by a human lung epithelial cell line (Fig. 5*B*) and to primary alveolar type II pneumocytes (19); in those cells, the analog was incorporated only by cells of the highest relative size.

Consistent with these observations, *group II* of the N12 human lung fibroblasts yielded the highest rate of accumulation by 8 days of culture begun immediately after separation by 1 G (Fig. 6). By *day 13* of culture, the rate of growth of *group I* had surpassed that of *group II*, but both *groups I* and *II* grew significantly faster than *group III*. As shown in Fig. 6, *inset*, cells of *groups I* and *II* increased in size by culture *day 13*, but those of *group III* did not. None of the three fibroblast groups reached confluence by *day 15* of culture (data not shown), and thus the slower growth rates of *group III* and eventually *group II* were unrelated to density arrest.

Fibroblast size, apoptosis, and α-actin expression. To determine the relationship between fibroblast phenotype, DNA fragmentation, and spontaneous apoptosis, unfractionated N12 cells were harvested at mid-log phase and subjected to ISEL of fragmented DNA (17). Microscopy of adherent cells (Fig. 7) revealed two populations of labeled cells: fibroblasts with moderate (Fig. 7, *A* and *B*) and high (Fig. 7, *C* and *D*) intensity of

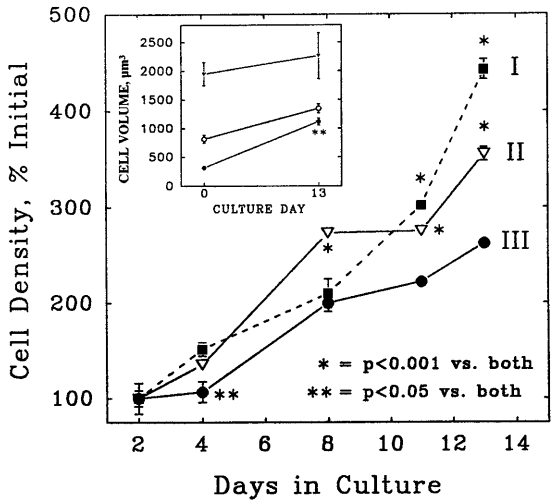

Fig. 6. Growth in primary culture of human lung fibroblasts separated by 1 G. Fibroblast *groups I*, *II*, and *III* defined in Fig. 3 were placed in primary culture in presence of 10% fetal bovine serum for 15 days. At the indicated days, cell number was estimated by WST-1 assay (see METHODS). Each point is mean ± SD; where not visible, error bars fall within symbols. *Inset*: cell volume measurements on isolated *groups I–III* on *days 0* and *13* of culture. Note increase in cell size in *groups I* and *II* but not in *group III*. Significant difference compared with both other groups on the same day of culture: $*P < 0.001$; $**P < 0.05$ (by ANOVA and Student-Newman-Keuls test).

ISEL labeling. Many labeled cells displayed condensation of the labeled chromatin, nuclear fragmentation (Fig. 7*D*), and blebs in the plasma membrane (Fig. 7*C*, arrow), indicative of late apoptosis (21). Immunofluorescence detection of α-SMA revealed both unlabeled cells (Fig. 7*E*, arrows) and cells labeled with the monoclonal antibodies to varying degrees (Fig. 7*F*, same field as Fig. 7*E*).

Flow cytometric analyses of FALS versus ISEL labeling (Fig. 8*A*) resolved both the moderately and highly labeled subsets, which comprised 30.9 and 4.9%, respectively, of the total fibroblast population. In parallel experiments, labeling of viable fibroblast preparations with the sensitive apoptosis marker annexin V (Fig. 8*B*) also discriminated moderately and highly labeled subsets, which were present in similar proportions. Although the moderate ISEL subset was composed of both mid-FALS (*group II*) and high-FALS (*group III*) fibroblasts, the high-ISEL and high-annexin V subsets were found to consist only of the large *group III* cells. Similar analyses (Fig. 8*C*) of FALS versus immunoreactivity to α-SMA antibodies revealed that α-SMA expression was also found only in *group III* fibroblasts.

However, double labeling for ISEL and α-SMA (Fig. 9) revealed that the two labels were not necessarily observed in the same cell. α-Actin-positive fibroblasts (Fig. 9, bracket) were found to be either unlabeled or positively labeled by ISEL as were α-SMA-negative cells. Conversely, both groups of ISEL-labeled cells (moderate and high; Fig. 9) were composed of either α-SMA-positive or -negative fibroblasts, as was the ISEL-negative population.

DISCUSSION

As discussed earlier by Bont et al. (2), unit gravity sedimentation (1 G) separates particles on the basis of size, independently of density. This method therefore offered a theoretically feasible approach to isolating the "large and flat" fibroblasts observed by our laboratory and previously by other investigators (1, 15, 23). We found that the method easily resolved subsets of differing volume (Fig. 2) and morphologies that were stable for up to 15 days in culture. With the exception of the smallest fibroblast subset (*fractions 25–30*), the cells of which were only slightly larger than nuclei, cell volume

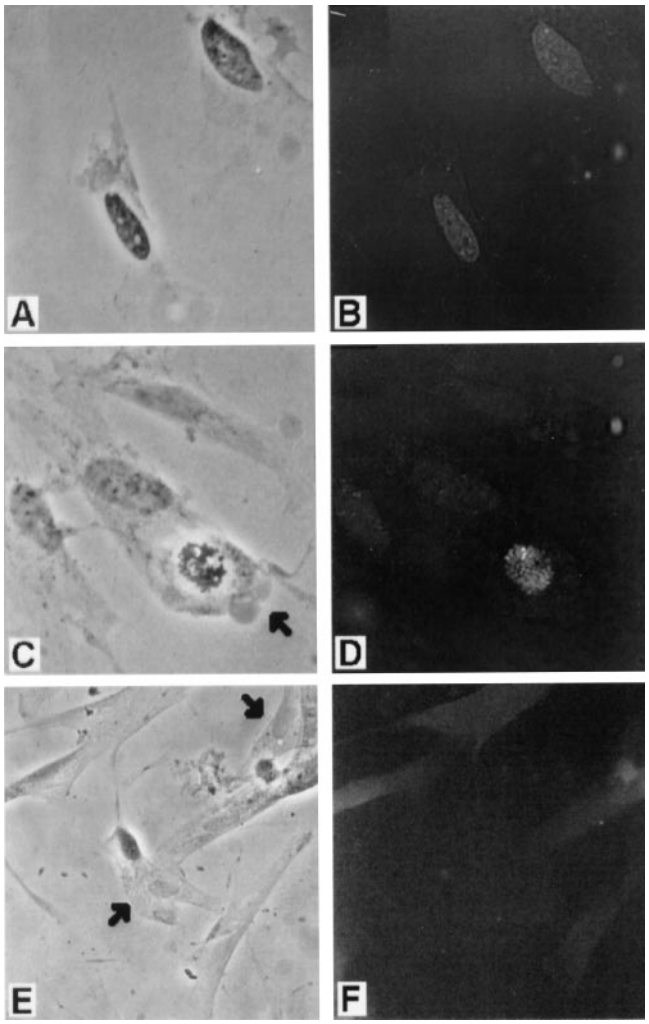

Fig. 7. In situ end labeling (ISEL) of fragmented DNA and immunofluorescence detection of α-smooth muscle actin (α-SMA) in primary human lung fibroblasts. Shown are phase-contrast (*A*, *C*, and *E*) and fluorescence (*B*, *D*, and *F*) images of the same fields of cells. N12 fibroblast strain was cultured to mid-log phase. Cells were labeled by a modified ISEL protocol (25) or with FITC-conjugated monoclonal antibodies to α-SMA (see METHODS). ISEL labeling of nuclei was observed as negative, moderate (*A* and *B*), or high intensity (*C* and *D*); some labeled cells displayed chromatin condensation and nuclear fragmentation (*D*) and blebbing of plasma membrane (*C*, arrow), indicative of late apoptosis (11, 21). Immunofluorescence detection of α-SMA (*E* and *F*) revealed occasional heavily labeled fibroblasts (*F*, *top left*), moderate labeling (*F*, *top*), and many unlabeled fibroblasts (*E*, arrows; compare with *F*). See Figs. 8 and 9 for FACS and imaging quantitations of ISEL and α-SMA.

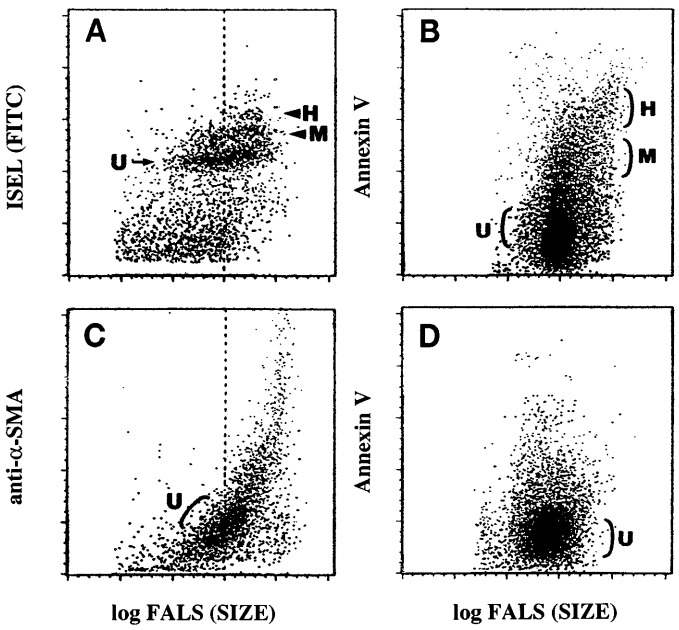

Fig. 8. Relationship of human lung fibroblast size to DNA fragmentation, annexin V binding, and α-SMA immunoreactivity. *A*: unfractionated primary N12 human lung fibroblasts were cultured to mid-log phase and harvested for FACS detection of cell size, measured as FALS vs. fragmented DNA detected by ISEL as described in Fig. 7. Note mid- to high-FALS profile of cells with moderate ISEL labeling (M), and high-FALS profile of fibroblasts with high ISEL labeling (H); compare FALS values of each to constant FALS marker at channel 150 (dotted line). U, unlabeled fibroblast population. M and H subsets comprised 30.9 and 4.9%, respectively, of total fibroblast population. *B*: unfractionated N12 cells in viable suspension were incubated with fluorescein-conjugated annexin V and analyzed 1 h later (see METHODS). *Populations M* and *H* comprised 21.1 and 3.2%, respectively, of total fibroblasts. *C*: N12 fibroblasts were cultured and harvested in the same way as in *A*; cells were incubated with FITC-conjugated monoclonal antibodies to α-SMA (anti-α-SMA; see METHODS) and subjected to FACS analysis of FALS vs. FITC fluorescence. Note high-FALS profile of cells with positive α-SMA labeling. Analysis was repeated 3 times with similar results. *D*: control annexin V-binding profile of viable suspension of A549 lung epithelial cells; <5% displayed positive binding.

correlated well with FALS; this result confirms that FALS will provide a reliable index of fibroblast size for future flow cytometric studies of subpopulation dynamics.

The observation that *group II* contained the greatest percentage of S and G_2/M phase cells (Fig. 4) and virtually all BrdU-positive cells (Fig. 5) agrees with the model of "balanced cell growth" discussed by Darzynkiewicz et al. (3). In that concept of cell cycle progression, quiescent cells entering the cell cycle must increase cellular RNA content (primarily ribosomal) and protein content (and thus cell size) to a value above some threshold level; reaching the threshold is a prerequisite to passage of the "restriction point," believed to reside at the G_1/S phase border (4). Within *group I* fibroblasts, the small cell size and paucity of S phase cells is consistent with the designation of this subset as quiescent but capable of proliferation.

This interpretation is also supported by the growth curves in Fig. 6; *group I* fibroblasts lagged behind *group II* in their rate of accumulation by 8 days of culture but surpassed both *groups II* and *III* by 13 days. The latter observation suggests that within *group I* competent fibroblasts entered the cell cycle between 8 and 13 days of culture, whereas many of the *group II* cells were already in the cell cycle at the time of 1 G separation. In support of this view, the small *group I* cells transformed into the larger *group II* phenotype during the 8- to 13-day culture interval, indicating that balanced cell growth was maintained after 1 G separation (Fig. 6, *inset*).

Group III, the largest fibroblasts, grew most slowly at all culture times (Fig. 6) and was among the two groups (*groups II* and *III*) that contained ISEL-labeled apoptotic cells (Figs. 7 and 8). These observations suggest that the slow rate of growth of *group III* may be the result of a high rate of spontaneous apoptosis relative to cell division. Although cells labeled by ISEL were found in both *groups II* and *III*, *group II* contained the highest proportion of S phase cells (Figs. 4 and 5); these would be expected to offset cell death by apoptosis, and the growth curves in Fig. 6 are consistent with this interpretation. In this regard, it is interesting to note that the low C1q-binding subset of human lung fibroblasts identified by Akamine et al. (1) also displayed a poor rate of growth in culture despite containing a higher percentage of cycling cells identified by flow cytometry. This paradox might also be explained by a higher rate of spontaneous apoptosis within this subpopulation, which exhibited the same morphological characteristics (large and flat) as *group III* of the present study. The methods described here will offer an ideal approach to addressing this issue. These methods will also be useful in examining the relationship of lipid inclusion bodies (15) to fibroblast phenotype when coupled with fluorescent lipophilic probes. The fibroblast strain studied here, however, did not contain significant numbers of lipid inclusions to permit such an analysis.

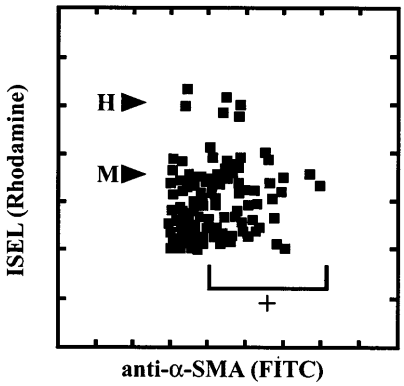

Fig. 9. Bivariate analysis of DNA fragmentation and α-SMA immunoreactivity in primary human lung fibroblasts. N12 fibroblast strain was cultured as described in Fig. 8. Adherent cells were subjected to double labeling for ISEL and α-SMA, each conducted as described in Fig. 7; quantitation of both labels was performed by image analysis (see *methods*). Bracket, α-SMA-positive (+) fibroblasts. M and H, same moderately and highly labeled cells, respectively, detected by ISEL as in Fig. 8. Note that ISEL labeling is found in both α-SMA-negative and -positive fibroblast populations.

The presence of both immunoreactivity to α-actin antibodies and ISEL labeling in *group III* suggested that fibroblast apoptosis might be associated with the acquisition of the myofibroblast phenotype. Such an association was suggested earlier (6) and was supported by the finding of apoptosis in myofibroblast populations within granulation tissue transforming to scar (7). Our double-labeling data (Fig. 9) argue against such an association because ISEL labeling was clearly observed in both α-actin-negative and -positive fibroblasts in comparable proportions. In addition, α-actin expression by primary isolates of rat lung mesenchymal cells has been observed not only in large "lacy" cells but also in a group of smaller, more tightly packed clones (13). Whether these discrepancies are due to species differences, cell culture conditions, or other factors awaits further investigation.

In summary, we describe a simple and reproducible unit gravity sedimentation method for the isolation of human lung fibroblast subsets in high yield on the basis of cell size. Kinetic and flow cytometric analyses identified three size subsets corresponding to young quiescent (*group I*), rapidly proliferating (*group II*), and large slow-growing (*group III*) groups. Under conditions of log-phase growth, only *group III* exhibited expression of α-SMA, but double-labeling studies indicated that both α-actin-positive and -negative cells were capable of spontaneous apoptosis. These results suggest that α-actin expression by lung fibroblasts does not necessarily precede or accompany a commitment to apoptosis. The ease and high yield of the method described will facilitate future investigation of the functions and interrelationships of known fibroblast subsets.

We thank the Department of Medicine, University of Illinois at Chicago, for administrative assistance in arranging the visit of Research Scholar C. Ramos of the Instituto Nacional de Enfermedades Respiratorias de Mexico (Tlalpan).

This work was supported by National Heart, Lung, and Blood Institute Grant HL-45136 to B. D. Uhal; the Women's Board Endowment to the Research and Education Foundation of the Michael Reese Medical Staff; and the Universidad Nacional Autonoma de Mexico.

Address for reprint requests: B. D. Uhal, Cardiovascular Institute, Michael Reese Hospital, 2929 S. Ellis Ave., Rm. 405KND, Chicago, IL 60616.

Received 14 April 1998; accepted in final form 10 August 1998.

REFERENCES

1. **Akamine, A., G. Raghu, and A. S. Narayanan.** Human lung fibroblast subpopulations with different Clq binding and functional properties. *Am. J. Respir. Cell Mol. Biol.* 6: 382–389, 1992.
2. **Bont, W. S., J. E. DeVries, M. Geel, A. Van Dongen, and H. A. Loos.** Separation of human lymphocytes and monocytes by velocity sedimentation at unit gravity. *J. Immunol. Methods* 29: 1–16, 1979.
3. **Darzynkiewicz, Z., H. Crissman, F. Traganos, and J. Steinkamp.** Cell heterogeneity during the cell cycle. *J. Cell. Physiol.* 113: 465–474, 1982.
4. **Darzynkiewicz, Z., T. Sharpless, L. Staiano-Coico, and M. R. Melamed.** Subcompartments of the G1 phase of cell cycle detected by flow cytometry. *Proc. Natl. Acad. Sci. USA* 77: 6696–6699, 1980.
5. **Derdak, S., D. P. Penney, P. Keng, M. E. Felch, D. Brown, and R. P. Phipps.** Differential collagen and fibronectin production by Thy 1+ and Thy 1− lung fibroblast subpopulations. *Am. J. Physiol.* 263 (*Lung Cell. Mol. Physiol.* 7): L283–L290, 1992.
6. **Desmouliere, A., and G. Gabbiani.** The role of the myofibroblast in wound healing and fibrocontractive diseases. In: *The Molecular and Cellular Biology of Wound Repair*. New York: Plenum, 1996, p. 391–423.
7. **Desmouliere, A., M. Redard, L. Darby, and G. Gabbiani.** Apoptosis mediates the decrease in cellularity during the transition between granulation tissue and scar. *Am. J. Pathol.* 146: 56–66, 1995.
8. **Fries, K. M., T. Blieden, R. J. Looney, G. D. Sempowski, M. R. Silvera, R. A. Willis, and R. P. Phipps.** Evidence of fibroblast heterogeneity and the role of fibroblast subpopulations in fibrosis. *Clin. Immunol. Immunopathol.* 72: 283–292, 1994.
9. **Gabbiani, G.** The biology of the myofibroblast. *Kidney Int.* 41: 530–532, 1992.
10. **Gorczyca, W., J. Gong, and Z. Darzynkiewicz.** Detection of DNA strand breaks in individual apoptotic cells by the in situ terminal deoxynucleotidyl transferase and nick translation assays. *Cancer Res.* 53: 1945–1951, 1993.
11. **Grasl-Kraup, B., B. Ruttkay-Nedecky, H. Koudelka, K. Bukowska, W. Bursch and R. Schulte-Hermann.** In situ detection of fragmented DNA fails to discriminate among apoptosis, necrosis and autolytic cell death: a cautionary note. *Hepatology* 21: 1465–1468, 1995.
12. **Kuhn, C., and J. McDonald.** The roles of the myofibroblast in idiopathic pulmonary fibrosis. *Am. J. Pathol.* 138: 1257–1265, 1991.
13. **Mitchell, J., J. Woodcock-Mitchell, L. Perry, J. Zhao, R. Low, L. Baldor, and P. Absher.** In vitro expression of the α-smooth muscle actin isoform by rat lung mesenchymal cells: regulation by culture condition and transforming growth factor-β. *Am. J. Respir. Cell Mol. Biol.* 9: 10–18, 1993.
14. **Pardo, A., and M. Selman.** Decreased collagenase production by fibroblasts derived from idiopathic pulmonary fibrosis. *Matrix Suppl.* 1: 417–448, 1992.
15. **Phipps, R. P., D. P. Penney, P. Keng, H. Quill, A. Paxhia, S. Derdak, and M. E. Felch.** Characterization of two major populations of lung fibroblasts: distinguishing morphology and discordant display of Thy 1 and class II MHC. *Am. J. Respir. Cell Mol. Biol.* 1: 65–74, 1989.
16. **Reif, A. E., and J. Allen.** The AKR thymic antigen and its distribution in leukemias and nervous tissues. *J. Exp. Med.* 120: 413–433, 1964.
17. **Sempowski, G. D., M. P. Beckmann, S. Derdak, and R. P. Phipps.** Subsets of murine lung fibroblasts express membrane-bound and soluble IL-4 receptors. Role of IL-4 in enhancing fibroblast proliferation and collagen synthesis. *J. Immunol.* 152: 3606–3614, 1994.
18. **Skalli, W., T. Schurch, R. Seemayer, D. Lagace, B. Montandon, P. Gabbinai, and G. Gabbiani.** Myofibroblasts from diverse pathologic settings are heterogeneous in their content of actin isoforms and intermediate filament proteins. *Lab. Invest.* 60: 275–285, 1989.
19. **Uhal, B. D., and M. D. Etter.** Type II pneumocyte hypertrophy without activation of surfactant biosynthesis after partial pneumonectomy. *Am. J. Physiol.* 264 (*Lung Cell. Mol. Physiol.* 8): L153–L159, 1993.
20. **Uhal, B. D., G. D. Hess, and D. E. Rannels.** Density-independent isolation of type II pneumocytes after partial pneumonectomy. *Am. J. Physiol.* 256 (*Cell Physiol.* 25): C515–C521, 1989.
21. **Uhal, B. D., I. Joshi, A. True, S. Mundle, A. Raza, A. Pardo, and M. Selman.** Fibroblasts isolated after fibrotic lung injury induce apoptosis of alveolar epithelial cells in vitro. *Am. J. Physiol.* 269 (*Lung Cell. Mol. Physiol.* 13): L819–L828, 1995.
22. **Uhal, B. D., and D. E. Rannels.** DNA distribution analysis of type II pneumocytes by laser flow cytometry: technical considerations. *Am. J. Physiol.* 261 (*Lung Cell. Mol. Physiol.* 5): L296–L306, 1991.
23. **Vande Berg, J. S., R. Rudolph, and M. Woodward.** Comparative growth dynamics and morphology between cultured myofi-

broblasts from granulating wounds and dermal fibroblasts. *Am. J. Pathol.* 114: 187–200, 1984.

24. **Vande Berg, J. S., R. Rudolph, and M. Woodward.** Growth dynamics of cultured myofibroblasts from human breast cancer and nonmalignant contracting tissues. *Plast. Reconstr. Surg.* 73: 605–618, 1984.
25. **Wijsman, J. H., R. R. Jonker, R. Keijzer, C. J. H. Van De Velde, C. J. Cornelisse and J. H. Van Dierendonck.** A new method to detect apoptosis in paraffin sections: in situ end-labeling of fragmented DNA. *J. Histochem. Cytochem.* 41: 7–12, 1993.
26. **Willis, R. A., A. K. Nussler, K. M. Fries, D. A. Geller, and R. P. Phipps.** Induction of nitric oxide synthase in subsets of murine pulmonary fibroblast: effect on fibroblast interleukin-6 production. *Clin. Immunol. Immunopathol.* 71: 231–239, 1994.